ORIGINAL PAPER

Semi-active tuned mass dampers under combined variable actions of friction forces and external disturbances

Enrico Zacchei[1,2] · Reyolando Brasil[3,4]

Abstract

Anti-seismic devices are employed to implement the best performance of the structures under earthquakes. In this paper, semi-active tuned mass dampers (SA-TMDs) are studied by considering several combinations of variable friction forces and external disturbances. The variable damping model is used, where the goal consists in estimating the external actions to find the best friction force for system dampening. In particular, general, sinusoidal, and Gaussian dynamic loadings are considered. To obtain the response of the structure and dampers, several numerical solutions have been implemented. Probabilistic and determines analyses have been also developed to study different damper characteristics. Results show that a SA-TMD can reduce the structure displacements up to ~70.0% indicating a good performance in controlling different oscillations. This technology not only preserves the integrity of a structure mitigating its vibrations but also improves the life of occupants and their safety and comfort. This is beneficial from the perspective of practical application, and it is an advancement with respect to this theme.

Keywords Semi-active control · Tuned mass dampers · Variable damping model · Earthquake engineering · Structural engineering

Introduction

Background

Technologies for the seismic protection of constructions and preventing "motion sickness" (Bekdaş et al. 2018) of residents are successfully employed in civil structures, and they have been studied in the recent years having undergone great development (Zacchei and Brasil 2022). These technologies are mainly divided into passive, active, semi-active control, and seismic isolators (Ciampi et al. 2009).

Responsible Editor: Murat Karakus

✉ Enrico Zacchei
   enricozacchei@gmail.com

1   Itecons, Coimbra, Portugal

2   University of Coimbra, CERIS, Coimbra, Portugal

3   Polytechnic School, University of São Paulo (USP), 380 Prof. Luciano Gualberto, São Paulo, SP, Brazil

4   Center for Engineering, Modeling and Applied Social Sciences, Federal University of ABC (UFABC), Alameda da Universidade s/n, São Bernardo do Campo, SP, Brazil

Passive controls are simple and efficient vibration absorbers. They act passively since they create reactive forces solely in response to the motion of the structure and they are not externally driven (OPCM 2005; SPES 2017). Their main problem is that they may not be suitable when the system is excited by a non-design earthquake (Chung et al. 2011; Lai et al. 2016). For instance, an extreme earthquake, difficult to prevent, with a long-period waveform may induce unexpected displacements (Zacchel et al 2017; Zacchei et al. 2018; Maddaloni et al. 2017; Chung et al. 2011).

The active controls have a great reduction of the structure response at the expense of large power consumption. They act as generating forces in the time domain; however, they may be instable and need an energy source, sensors, servo-valves, time controllers, and computers to define these forces (Jiang 2018).

Seismic isolations reduce the energy transmitted from the external loads to the structure (Bagheri and Rahmani-Dabbagh 2018; Lazarek et al. 2018) by, e.g. (i) increasing the structural period to decrease the spectral accelerations on the structures (CEN 2004, 2008); (ii) reducing inertial external forces by reducing the participating mass; and (iii) increasing the damping ratio (Ciampi et al. 2009).

Reducing the mass can also avoid twisting effects, e.g. in planimetric/altimetric asymmetric structures and historical buildings (Castellano et al. 2001).

Isolators, passive, and active devices are applied for bridges, buildings, and historical structures as shown in Castellano and Infanti (2009), Shi et al. (2018b), and Lai et al. (2016). In general, passive controls and isolators are the most used.

For instance, in the Rion-Antirion Bridge in Greece, fluid viscous dampers have been applied. In Venezuela, the Caracas-Tuy Medio Railway line has more than 1500.0 steel hysteretic dampers isolators. In Algeria and in Italy, there are more than 2300.0 high-damping elastomeric isolators (Castellano and Infanti 2009). Regarding buildings, two examples in Italy are the Hospital Del Mare with 327.0 elastomeric isolators installed between piles and super-structure and the Cappuccini School with several dissipative bracing. Interesting cases, where a tuned mass damper (TMD) has been applied to reduce the oscillations, are the Taipei 101 Skyscraper in Taiwan (Castellano and Infanti 2009) and the CN tower in Toronto, Canada (Chang et al. 2018; Lai et al. 2016). Finally, for historical structures, in S. Francesco Basilica, Assisi in Italy, metal devices have been applied. In the USA, rubber isolators were first used in the Salt Lack City and County Building (Castellano et al. 2001).

Also, these technologies can be used in other fields, for instance, (i) in industrial engineering, for storage tanks (Ciampi et al. 2009), offshore platform for wind turbines (Sun and Jahangiri 2018; Jiang 2018; Hussan et al. 2018), or offshore drilling structures for oil and gas extraction (Wu et al. 2018; Sanchez et al. 2017); and (ii) in mechanical engineering, for vehicles (Trikande et al. 2017). Different aspects have been studied by researchers, such as the dynamic soil-structure interactions (Salvi et al. 2018; Jabary and Madabhushi 2018), interactions and collision with adjacent constructions (Basili et al. 2013), and multiple TMDs effects (Wen et al. 2018; Kim and Lee 2019, 2018).

In Wen et al. (2018), it was proposed the effectiveness of an innovative multiple tuned mass damper (MTMD) mitigation strategy for potential transformer by using analytical and computational finite element methods.

In this paper, the semi-active tuned mass dampers (SA-TMDs) are studied since they offer the reliability of passive devices and maintain the versatility of active devices. They are based on mechanisms like the passive controls providing a passive force but considering the mechanical characteristics in the time domain. SA-TMDs use the advantages of a controlled force without the drawback of active systems (i.e. without large energies) (Fitzgerald et al. 2018). They are small and low-cost; therefore, they have little interferences to the structure.

However, like active control, they need sensors and computers to receive the sensors' signals and control the actuators and forces (Wang et al. 2021).

SA-TMDs are applied to control the vibration of flexible and low-damping structures under different excitations such as vehicle vibrations, wind, and earthquakes as shown in Chung et al. (2013). Several studies are available in the literature on SA-TMDs, which are divided with respect to different mechanical systems, e.g. with variable friction (Chung et al. 2011; Gaul and Becker 2014; Shi et al. 2018a; Pinkaew and Fujino 2001), variable stiffness (Nagarajaiah and Sonmez 2007; Nagarajaiah and Varadarajan 2005; Eason et al. 2013), magnetorheological (MR) dampers (Oliveira et al. 2015; Gu et al. 2017a, 2017b; Xia et al. 2016; Bahar et al. 2010; Aggumus and Cetin 2018; Zapateiro et al. 2009), and energy transition controls (Shuliang et al. 2011).

Other studies show other types of SA-TMDs, for example by using bearing made of super low-cost recycled elastomers and reinforced with fibre sheets (Maddaloni et al. 2017) and sloped rolling-type isolation devices (Chen and Wang 2017). Applications for steel structures also have been studied (Lorenz et al. 2006; Gaul et al. 2004).

In Chung et al. (2013), the numerical validation of the SA-TMD has been carried out by using several types of loadings, e.g. sinusoids with different frequencies, and random loadings.

Finally, in Elias and Matsagar (2018), Jabary and Madabhushi (2018), and Wang et al. (2018b), it was studied how the mobility and the different positioning of the damper affect the structure response. In Wang et al. (2018a) and Van Til et al. (2019), the effect of the presence of vertical barriers has been treated; in fact, when a SA-TMD exceeds the gap between its initial position and the barrier, the damper impacts on the barrier providing supplementary energy dissipation.

Motivation of this study

As mentioned, in this paper, the SA-TMD has been studied to.

1. Implement new standard methodologies to guarantee high-grade products and support structural engineers in acquiring the knowledge to select the most effective solution. As stated in Medeot (2017), European code [19] "represents the most complete and up-to-date document" on anti-seismic devices (see Table 6 in Annex A); however, SA-TMDs are not mentioned.

Figure 1 shows the possible types of controls (Lu et al. 2018a, 2018b). A hybrid control can combine passive with semi-active systems (Bahar et al. 2010). However, this distinction is not well defined since in Lai et al. (2016), active TMDs are called "hybrid mass dampers", and in Medeot
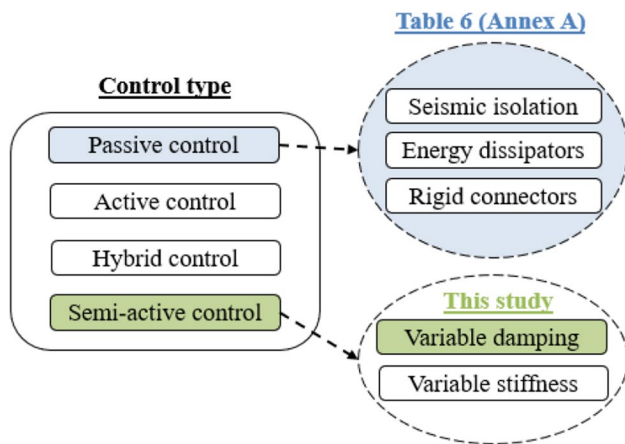
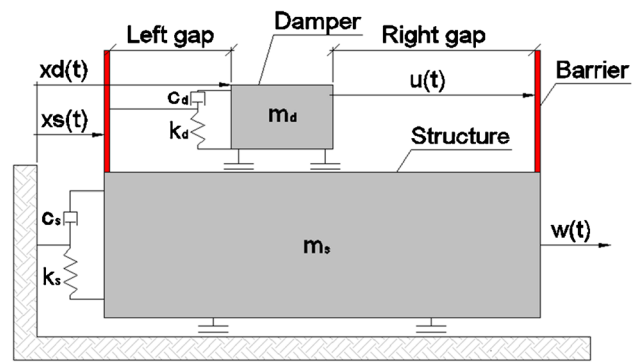**Fig. 1** Scheme of the control types (Ciampi et al. 2009) (in green the control studied in this paper)

Fig. 2 SDOF structure model with an SA-TMD. The mass damper, between two vertical barriers, is placed on the structure (Chung et al. 2013; AutoCAD 2010)

(2017), all the pre-existing devices combined one with each other are called "hybrids". Table 6 (Annex A) lists the most used anti-seismic devices (i.e. passive control and isolators).

2. Improve its limited use with respect to other devices since it provides modern and high-tech approaches. In fact, in Wang et al. (2021), it is stated that SA-TMDs "can identify the structural instantaneous vibrational frequency and retune itself in real time". As discussed in Maddaloni et al. (2017) and Van Til et al. (2019), these applications need more studies to improve the performances and sustainability of the structures.

The key problem of an SA-TMD is the definition of the control force, which is difficult to be estimated a priori. For this, in this paper, different multi-harmonics to simulate the external dynamic actions are adopted (this approach has been also adopted in Ma et al. (2019) and Zacchei and Brasil (2022) to simulate the seismic source). Then, numerical analyses have been implemented to find optimal solutions in terms of structural displacements. Their reduction helps improving the life of occupants and "leads to preserving the integrity of the structure" as mentioned in Zapateiro et al. (2009).

Semi-active tuned mass damper (SA-TMD) model

The SA-TMD model is formed by a structure, called "primary structure", fixed on the base and a mass "damper" (or "secondary structure"). Both structure and mass damper have a single-degree-of-freedom (SDOF).

Figure 2 shows this configuration where the structure is placed below the mass damper, which can move between a certain limit imposed by two vertical barriers (i.e. end stop mechanism (Wang et al. 2018a; Til et al. 2019)). Barriers should reduce the SA-TMD motions, the installation space thus its costs (Til et al. 2019).

The equation of motion, in the time t, of the system is (Chung et al. 2013)

$$\mathbb{M}\ddot{x}(t) + \mathbb{C}\dot{x}(t) + \mathbb{K}x(t) = \mathbb{b}u(t) + \mathbb{e}w(t) \tag{1}$$

where $\mathbb{M} \in R^{n \times n}$, $\mathbb{C} \in R^{n \times n}$, and $\mathbb{K} \in R^{n \times n}$ are the inertia, damping, and stiffness matrices, defined, respectively, as

$$\mathbb{M} = \begin{bmatrix} m_d & 0 \\ 0 & m_s \end{bmatrix} \tag{2}$$

$$\mathbb{C} = \begin{bmatrix} c_d & -c_d \\ -c_d & c_s + c_d \end{bmatrix} \tag{3}$$

$$\mathbb{K} = \begin{bmatrix} k_d & -k_d \\ -k_d & k_s + k_d \end{bmatrix} \tag{4}$$

where the three coefficients $m_i > 0$, $c_i > 0$, and $k_i > 0$ are the masses, damping, and elastic stiffness coefficients, respectively. The subscripts s and d refer to the structures and mass damper, respectively.

The function of k_d is to distribute the energy from the primary to the secondary structure, whereas c_d dissipates this energy; for this, the secondary structure can be considered as a damper.

The components of $x(t) = \left[x_d(t), x_s(t)\right]^T \in R^n$ represents the displacements, where the variables $\dot{x}(t)$ and $\ddot{x}(t)$ are the first and second time derivate of x, respectively. Matrices $\mathbb{b} = [1, -1]^T \in R^n$ is the variable friction force location vector, and $\mathbb{e} = [0, 1]^T \in R^n$ is the external disturbance location vector. Finally, $u(t)$ is a variable friction force, and $w(t)$ is

the external disturbance. The system is forced kinematically by springs k_i and $w(t)$.

Equation (1) in a first-order state-space form can be expressed as

$$\dot{z}(t) = \mathbb{A}z(t) + \mathbb{B}u(t) + \mathbb{E}w(t) \tag{5}$$

where $z(t) = [x(t), \dot{x}(t)]^T \in \mathbb{R}^n$ is the state vector, $\mathbb{B} = [0, \mathbb{M}^{-1}\mathbb{b}]^T \in \mathbb{R}^n$ is the state-space variable friction force location vector, $\mathbb{E} = [0, \mathbb{M}^{-1}\mathbb{e}]^T \in \mathbb{R}^n$ is the state-space external disturbance location vector, and the system matrix $\mathbb{A} \in \mathbb{R}^n$ is

$$\mathbb{A} = \begin{bmatrix} 0 & I \\ -\mathbb{M}^{-1}\mathbb{K} & -\mathbb{M}^{-1}\mathbb{C} \end{bmatrix} \tag{6}$$

In other words, $\mathbb{A} \in \mathbb{R}^{n \times n}$ denotes the system matrix composed of the mass, damping, and stiffness matrices, whereas $\mathbb{B}$ and $\mathbb{E}$ represent the distribution matrices of the control forces and the excitations, respectively.

The exact solution of Eq. (5) is

$$z(t) = e^{(\mathbb{A}t)}c_1 + e^{(\mathbb{A}t)} \int_1^t e^{-(\mathbb{A}t)}(\mathbb{B}u(t) + \mathbb{E}w(t))dt \tag{7}$$

where c_1 is an arbitrary constant of integration.

Equation (5) provides some solutions including sums and integrals that are difficult to be carried out directly. Therefore, some variables substituted by t are used. In this sense, Eq. (7) can be also developed in the discrete-time state-space form (Lu et al. 2004; Lai et al. 2016).

Under the non-state-space form (i.e. $z(t) \rightarrow$ non-state vector and A = B = E = 1), for initial condition $z(0) = 0$ and $u(t) = w(t) = \{\cos(t), \sin(t)\}$, it is possible to plot Eq. (7) trend as shown in Fig. 3.

An ideal control of this model could be indirectly achieved by adjusting mechanical parameters such as

Fig. 3 Trends of Eq. (7) in a non-state-space form

stiffness and/or damping. For this, SA-TMDs can be divided into two sub-models: (i) damping model (i.e. $u(t) \neq 0$, used in this work) and (ii) stiffness model (i.e. $u(t) = 0$, $k(t) \neq 0$). The former is treated in the "Variable damping model" section, whereas the latter basically consists in using, for instance, a time varying stiffness of the device as (Nagarajaiah and Varadarajan 2005; Chandiramani 2016):

$$k(t) = k_e \cos^2(\theta(t)) \tag{8}$$

where k_e is spring's constant stiffness, and $\theta(t)$ is the time-varying angle between k_e and the axis of the device direction, which reaches a maximum value for $\theta(t) = 0$ and a minimum value for $\theta(t) = \pi/2$ (for more details, see (Nagarajaiah and Varadarajan 2005; Chandiramani 2016)). $k(t)$ is included in the stiffness matrices $\mathbb{K}$ in Eq. (1) representing the internal forces of the system (Nagarajaiah and Sonmez 2007). As shown in Eason et al. (2013), in real applications, the stiffness tuning is achieved by a feedback control system, which monitors the structural response, calculates the dominant frequency of the excitation, and thus adjusts the stiffness.

Finally, Eq. (1) can be also represented in terms of energies (Medeot 2017). In this sense, it is possible to define the performance of the dynamic system by calculating the energy dissipated from devices and the energy input from external disturbances. Thus, the performance is the portion of the energy input that the system can dissipate.

Considering Eq. (1), the relative energy balance of the system between internal and external energies is defined as (Basili et al. 2013)

$$E_k(t) + E_d(t) + E_e(t) = E_u(t) + E_w(t) \tag{9}$$

where $E_k(t)$ is the kinetic energy, $E_d(t)$ is the energy dissipated by dampers, $E_e(t)$ is the elastic energy, $E_u(t)$ is the energy of variable friction forces, and $E_w(t)$ is the energy of external disturbances.

Variable damping model

The goal of this variable damping model is that the friction force to be like the desired control force. This model is an alternative strategy for dissipation the external excitations under specific configurations (Chung et al. 2011; Shi et al. 2018a; Lu et al. 2004).

Figure 4 shows a possible configuration of a friction system introduced in Shih and Sung (2021a, b). The main components are the bevel casting tube, switching tube, and locking steel ball linked with a cover plate by an internal spring. The internal mechanisms of this device are not treated in this study; here, only the output $u(t)$ form is studied. Basically, the general mechanism is divided into three phases: (i) registration of the external actions $w(t)$; (ii) processing of $w(t)$ by SA-TMD; and (iii) releasing of the $u(t)$ output on the
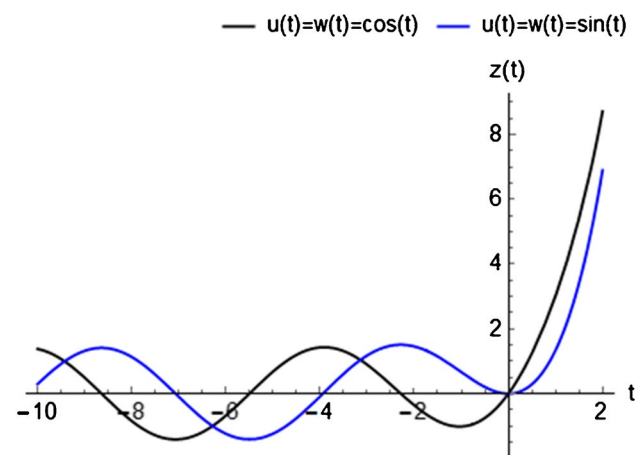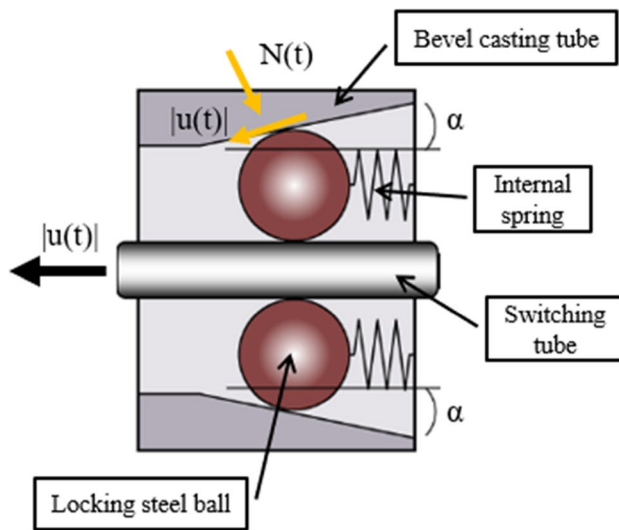
Fig. 4 Friction force system (modified from Shih and Sung 2021a)

structure to reduce its response (for more details, see (Shih and Sung 2021b)).

The force balance of the α/2 angle in the horizontal directions is

$$N(t)\sin\left(\frac{\alpha}{2}\right) = |u(t)|\cos\left(\frac{\alpha}{2}\right) \quad (10)$$

where the friction force $u(t)$, which is controlled indirectly by the normal friction force $N(t)$, is defined by Coulomb's model as (Chung et al. 2011)

$$\begin{cases} |u(t)| \leq \mu N(t) & \text{for } \dot{x}_s(t) = 0 \\ u(t) = \mu N(t)\text{sgn}(\dot{x}_s(t)) & \text{for } \dot{x}_s(t) \neq 0 \end{cases} \quad (11)$$

where μ is the friction coefficient of the force defined as $\tan(\alpha/2)$, and $|\cdot|$ is the absolute value. $\text{sgn}(\cdot)$ indicates that the control force produced by a variable damper is opposite to the direction of the current damper motion (i.e. passive resistance) (Lu et al. 2004). $u(t)$ in Eq. (11) is placed in the right-hand side of Eq. (1); therefore, it represents an external force.

As already mentioned, the definition of $u(t)$ is the problem key, which is difficult to be estimates a priori since $w(t)$ is unknown. For this, several cases have been generated as explained in the "Input motions" section.

Input motions

Three types of non-stationary loadings are considered: general, sinusoidal, and Gaussian dynamic loading. A general dynamic loading simulates irregular and aleatory time-histories (THs), which can be used to represent, e.g.

earthquakes, wind, machines' vibrations, and aerodynamic loads (Luzi et al. 2020). A sinusoidal harmonic loading can be used to simulate a more regular trend, e.g. temperature, humidity, long waves, sloshing, and convective pressures (Chung et al. 2013). Finally, Gaussian loadings could represent, e.g. impulsive actions, concentrated forces, and jumping excitations.

By considering these three loads, Eq. (1) becomes

$$\mathbb{M}\ddot{x}(t) + \mathbb{C}\dot{x}(t) + \mathbb{K}x(t) = \mathbb{b} \begin{Bmatrix} A_u \sum_{1=1}^{N} \sin(\omega_i t + \phi_i) \\ A_u \sin(t) \\ A_u e^{-t^2} \end{Bmatrix} + \mathbb{e} \begin{Bmatrix} A_w \sum_{1=1}^{N} \sin(\omega_i t + \phi_i) \\ A_w \sin(t) \\ A_w e^{-t^2} \end{Bmatrix}$$

$$(12)$$

where A_u and A_w are the amplitude of the force $u(t)$ and $w(t)$, respectively, ω_i is the circular frequency, ϕ_i is the random phase between 0 and 2π, and N is the arbitrary number of harmonic components.

Materials and methods

Materials

The used data regard deterministic and random values. Some pseudo-random parameters correspond to the damper data, whereas the structure data are imposed. The key values for the analysis are the mass, period, and damping ratio of the structure and the mass damper. The goal is to obtain a ratio $\mu_r \approx f_r \approx 1.0\%$ (Eq. (13)) as suggested in Chung et al. (2013) and Jabary and Madabhushi (2018), which provides the optimum damper response as suggested in Chung et al. (2013).

To define several values of T_d near to T_s, the stochastic Monte Carlo simulation (MCS) is performed. It generates pseudo random variables (RVs) within a predefined range where each parameter follows an adopted probability density function (PDF) (Su and Xu 2014; Hu et al. 2016). MCS consists in choosing an RV with a probability distribution in the range RV_{min} to RV_{max} up to a list of random values N_s. Here, the used range is $-0.50 \leq RV \leq 0.50$ with $N_s = 1.0 \times 10^6$ (Zacchei and Nogueira 2021).

Figure 5 shows MCS points (Fig. 5a) for T_d and the normal PDFs for the three dampers (Fig. 5b).

Table 1 and Fig. 6 show the adopted data of the structure and dampers.

Two dimensional mass, μ_r, and frequency, f_r, ratio are introduced to standardise the structure-damper system (Elias and Matsagar 2018; Salvi et al. 2018):

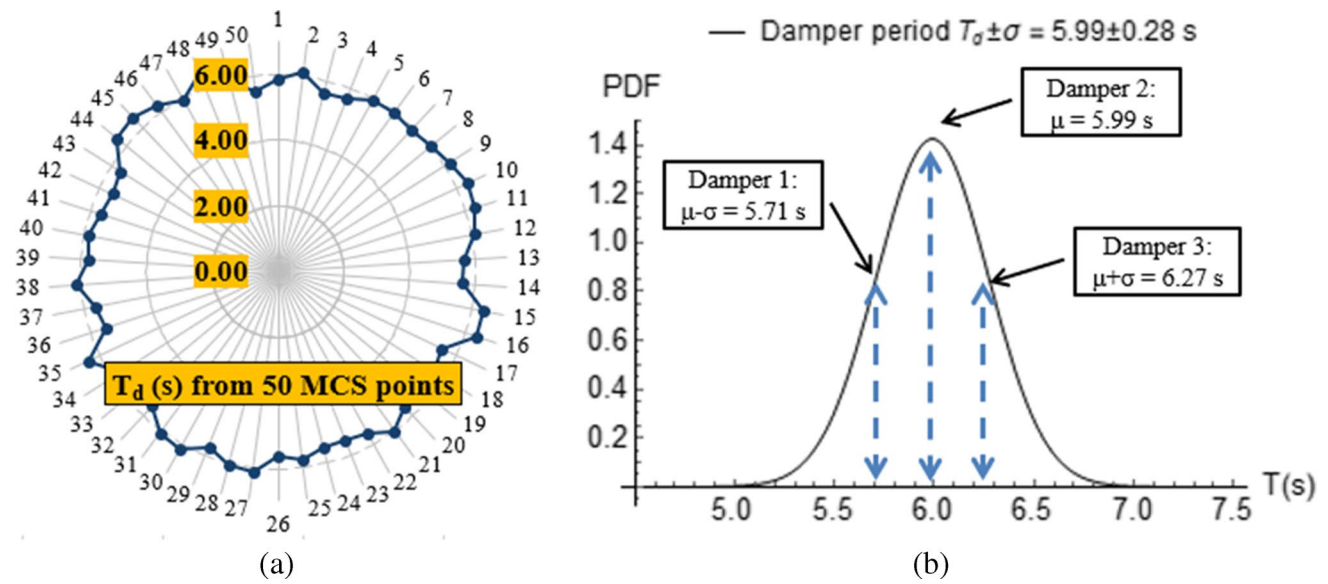$$f_r = \frac{f_d}{\Omega_{s,j}}, \mu_r = \frac{m_d}{\sum_{j=1}^{n} m_{s,j}} \quad (13)$$

Fig. 5 MCS results: **a** T_d values for only 50.0 points generated by MCS; **b** PDF for dampers T_d

Table 1 Adopted data of the structure and dampers

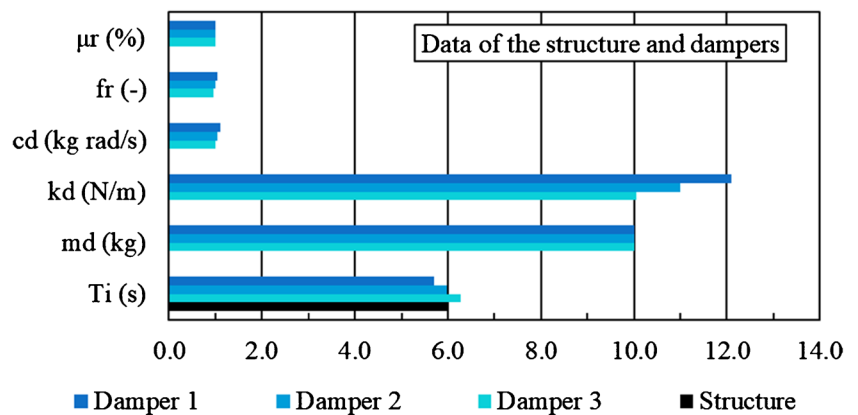| Parameter	Value
Structure mass, m_s (kg)	1.0×10^3 [a]
Structure damping ratio, ξ_s (%)	2.0 (Chung et al. 2013)
Structure period, T_s (s)	6.0 [b]
Structure stiffness, k_s (N/m)	1096.62 *
Structure damping, c_s (kg×rad/s)	41.88 *
Damper mass, m_d (kg)	0.01×10^3 (=1.0% of m_s) [a] (Jabary and Madabhushi 2018)
Damper damping ratio, ξ_d (%)	5.0 (CEN 2004, 2008)
Damper period, $T_d \pm \sigma$ (s)	5.99 ± 0.28 [b]

*Estimated value

[a] $\mu_r = 1.0\%$ (see Eq. (13)). Equation (2) is explicated as $\mathbb{M} = \begin{bmatrix} 0.01 & 0 \\ 0 & 1.0 \end{bmatrix} \times 10^3 \text{kg}$

[b] f_r ranges between 0.95 and 1.05 (see Eq. (13))

where f_d is the mass damper frequency ($= 1/T_d$) and $\Omega_{s,j} = \Omega_{s,1}, \ldots, \Omega_{s,n}$ ($= 1/T_{s,1}, \ldots, 1/T_{s,n}$) is the selected modal frequency of the structure corresponding to the mode j. A possible criterium to distribute the damper masses on the structure is carrying out the modal analysis (Elias and Matsagar 2018; Wu et al. 2011).

The structural values in Table 1 refer to the first mode of vibration since the control of the only lower modes is usually enough to mitigate the vibrations. The used values should represent in a realistic way the system in accordance with the literature (Chung et al. 2011; Eason et al. 2013; Kim and Lee 2019; Lu et al. 2018b) and design recommendations (Kim and Lee 2018). In general, for civil structures, it is usually assumed $\mu_r < 10.0\%$ (Jabary and Madabhushi 2018) and $\xi_d > \xi_s$ (CEN 2004, 2008; Shi et al. 2018a). However, ξ_s might not considered adequately some complex parameters as the material heterogeneity and the influence of the structural and
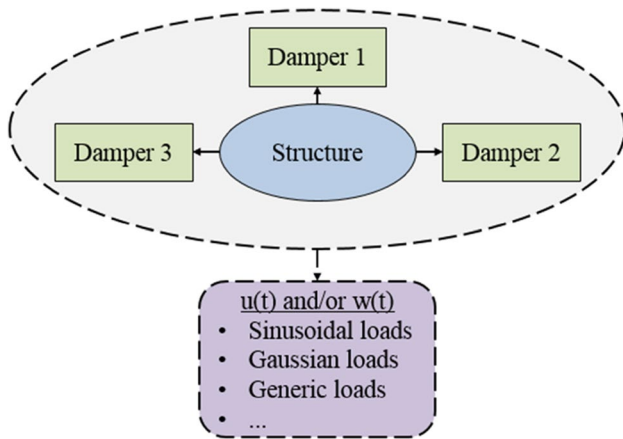
Fig. 6 Adopted data for the structure and dampers

Fig. 7 General configuration of the combinations adopted in this study

Table 2 Data of the three dampers

	T_d (s)	k_d (N/m) [a]	c_d (kg × rad/s) [b]
Damper 1	5.71	12.10	1.10
Damper 2	5.99	11.0	1.04
Damper 3	6.27	10.04	1.0

[a]By Eq. (4), $\mathbb{K}(N/m)$ is $\begin{bmatrix} 12.10 & -12.10 \\ -12.10 & 1108.72 \end{bmatrix}$, $\begin{bmatrix} 11.0 & -11.0 \\ -11.0 & 1107.62 \end{bmatrix}$, and $\begin{bmatrix} 10.04 & -10.04 \\ -10.04 & 1106.66 \end{bmatrix}$, for the dampers 1, 2, and 3, respectively
[b]By Eq. (3), $\mathbb{C}(kg \times rad/s)$ is $\begin{bmatrix} 1.10 & -1.10 \\ -1.10 & 42.98 \end{bmatrix}$, $\begin{bmatrix} 1.04 & -1.04 \\ -1.04 & 42.92 \end{bmatrix}$, and $\begin{bmatrix} 1.0 & -1.0 \\ -1.0 & 42.88 \end{bmatrix}$, for the dampers 1, 2, and 3, respectively

non-structural elements (Zacchei et al. 2020), whereas ξ_d can be estimated more easily since dampers are construct in laboratory, their sizes are small, and the material is homogeneous.

Figure 7 shows the schematic configuration of this study: three types of dampers with different period ratios are adopted to evaluate the damping effectiveness on the structure. Table 2 lists the characteristics of these dampers where T_d is generated by MCS, which provide semi-probabilistic parameters, i.e. k_d and c_d (Elias and Matsagar 2018).

Finally, regarding the input motions (Eq. (12)), the following values are adopted: $A_u = 10.0$ N, $A_w = 100.0$ N, and $N = 100.0$. Each simulation was set up such that the structure undergoes ~400.0 cycles of oscillation.

Methodology

Numerical solutions

Numerical simulations have been carried out to obtain the design parameters for the structure and dampers. By expanding Eq. (5), we obtain

$$\begin{bmatrix} \dot{x}(t) \\ \ddot{x}(t) \end{bmatrix} = \begin{bmatrix} 0 & I \\ -\mathbb{M}^{-1}\mathbb{K} & -\mathbb{M}^{-1}\mathbb{C} \end{bmatrix}\begin{bmatrix} x(t) \\ \dot{x}(t) \end{bmatrix} + \begin{bmatrix} 0 \\ \mathbb{M}^{-1}\mathbb{b} \end{bmatrix}\begin{bmatrix} u(t) \\ u(t) \end{bmatrix} + \begin{bmatrix} 0 \\ \mathbb{M}^{-1}\mathbb{e} \end{bmatrix}\begin{bmatrix} w(t) \\ w(t) \end{bmatrix}$$
(14)

Considering the second line of Eq. (14), which represents the accelerations $\ddot{x}(t)$, we obtain

$$\begin{bmatrix} \ddot{x}_d(t) \\ \ddot{x}_s(t) \end{bmatrix} = -\begin{bmatrix} m_d & 0 \\ 0 & m_s \end{bmatrix}^{-1}\begin{bmatrix} k_d & -k_d \\ -k_d & k_s+k_d \end{bmatrix}\begin{bmatrix} x_d(t) \\ x_s(t) \end{bmatrix}$$
$$-\begin{bmatrix} m_d & 0 \\ 0 & m_s \end{bmatrix}^{-1}\begin{bmatrix} c_d & -c_d \\ -c_d & c_s+c_d \end{bmatrix}\begin{bmatrix} \dot{x}_d(t) \\ \dot{x}_s(t) \end{bmatrix}$$
$$+\begin{bmatrix} m_d & 0 \\ 0 & m_s \end{bmatrix}^{-1}\begin{bmatrix} 1 \\ -1 \end{bmatrix}\begin{bmatrix} u(t) \\ u(t) \end{bmatrix} + \begin{bmatrix} m_d & 0 \\ 0 & m_s \end{bmatrix}^{-1}\begin{bmatrix} 0 \\ 1 \end{bmatrix}\begin{bmatrix} w(t) \\ w(t) \end{bmatrix}$$
(15)

of which two partial differential equations (PDEs) with respect to $\ddot{x}_s(t)$ and $\ddot{x}_d(t)$ are obtained (Shi et al. 2018a):

$$\ddot{x}_s(t) = \frac{k_d}{m_s}x_d(t) - \frac{(k_d+k_s)}{m_s}x_s(t) + \frac{c_d}{m_s}\dot{x}_d(t) - \frac{(c_d+c_s)}{m_s}\dot{x}_s(t) - \frac{1}{m_s}u(t) + \frac{1}{m_s}w(t)$$
(16)

$$\ddot{x}_d(t) = -\frac{k_d}{m_d}x_d(t) + \frac{k_d}{m_d}x_s(t) - \frac{c_d}{m_d}\dot{x}_d(t) + \frac{c_d}{m_d}\dot{x}_s(t) + \frac{1}{m_d}u(t)$$
(17)

In this study, Eqs. (16) and (17) are developed using Hermite polynomials (HPs) (Dattoli et al. 1998) by Mathematica software (Wolfram Mathematica 2017). An HP with the non-negative degree n in time t ($t \in R$) is specified by the series (Dattoli 2000):

$$H_n(t) = n! \sum_{r=0}^{\left[\frac{n}{2}\right]} \frac{(2t)^{n-2r}(-1)^r}{(n-2r)!r!}$$
(18)

As known, Eq. (18) provides the exact solution of a second-order homogeneous PDE (in the classical form) as shown in Yari and Mirnia (2021) and Abramowitz and Stegun (1965). However, Eqs. (16) and (17) present some differences with respect to the classical form (e.g. they are not homogeneous); therefore, it is necessary to define determined initial conditions (i.c.) to avoid arbitrary constants during the numerical integrations. Thus, the structure and damper displacements with the i.c. are described by

$$x_s(t) \rightarrow H_{n,s}(t), \dot{x}_s(t) \rightarrow H'_{n,s}(t), \ddot{x}_s(t) \rightarrow H''_{n,s}(t) \text{ with i.c.} : x_s(0) = 0, \dot{x}_s(0) = 0$$
$$x_d(t) \rightarrow H_{n,d}(t), \dot{x}_d(t) \rightarrow H'_{n,d}(t), \ddot{x}_d(t) \rightarrow H''_{n,d}(t) \text{ with i.c.} : x_d(0) = 0, \dot{x}_d(0) = 0$$
(19)

Fig. 8 Flowchart of the analysis (main steps)
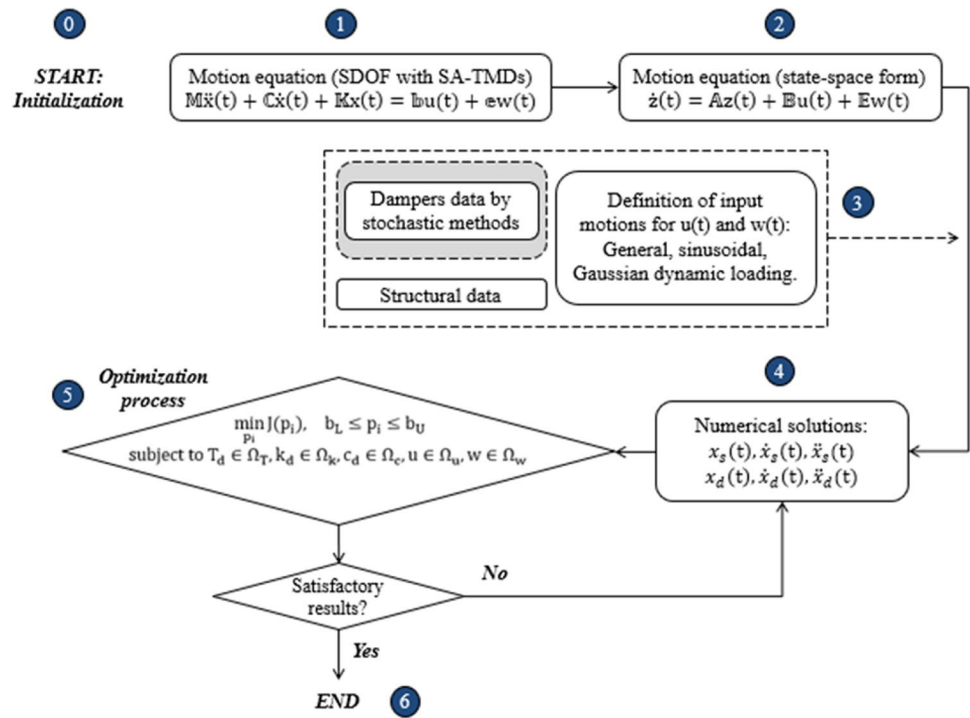
The process consists in finding the numerical solutions to a set of PDEs with several unknown functions x_j that depend on one or more independent variables t_j. Numerical PDEs represent solutions for the functions x_j by "interpolating function" (IF), which is the HP interpolation defined as a generalisation of linear interpolation (Eq. (18)). The IF provides approximations to the x_j over the range of values t_{initial} to t_{final} for the independent variables t_j. The process starts with a value of t_j, and then it takes a sequence of steps, trying to cover the whole range t_{initial} to t_{final} (Mathematica 2017).

Optimization process

The goal of the optimization process consists in minimising the displacements, velocities, and accelerations of the primary structure and SA-TMDs under different types of excitations. There are different optimization strategies and objective functions as shown in Nagarajaiah and Varadarajan (2005), Elias and Matsagar (2018), and Salvi et al. (2018). Here, the following problem is used, with the parameters defined in a domain Ω (e.g., Ω_T refers to the parameter T) (Salvi et al. 2018):

$$\begin{cases} \min_{p_i} J(p_i) \\ \text{for} \, b_L \leq p_i \leq b_U \\ \text{subject to} \, T_d \in \Omega_T, k_d \in \Omega_k, c_d \in \Omega_c, u \in \Omega_u, w \in \Omega_w \end{cases}$$

(20)

where $J(p_i)$ is set as the objective function of the variables p_i; b_L and b_U are the lower and upper bound of the optimization variables, respectively.

Since several combinations have been carried out, it is useful to consider a root mean square (RMS) defined for n values by

$$\text{RMS} = \sqrt{\frac{1}{n} \sum_{i=1}^{n} p_i^2}$$

(21)

Figure 8 shows the flowchart of the general methodology highlighting the main $5 + 2$ steps from the start (step 0) to the end (step 6). They consist in (1) description of the mathematical model (Eq. (1)); (2) transformation of the model in a state-space form (Eq. (5)); (3) definition of the input data by deterministic and probabilistic approaches; (4) developing numerical solutions; (5) choice of the optimization criteria and plotting of the results. If the results non are satisfactory, it is possible to adjust the i.c., b_L, b_U, and/or other parameters.

Analyses and results

Structure and dampers response

From Eqs. (16) and (17), the response in terms of displacements, velocities, and accelerations for the structure and
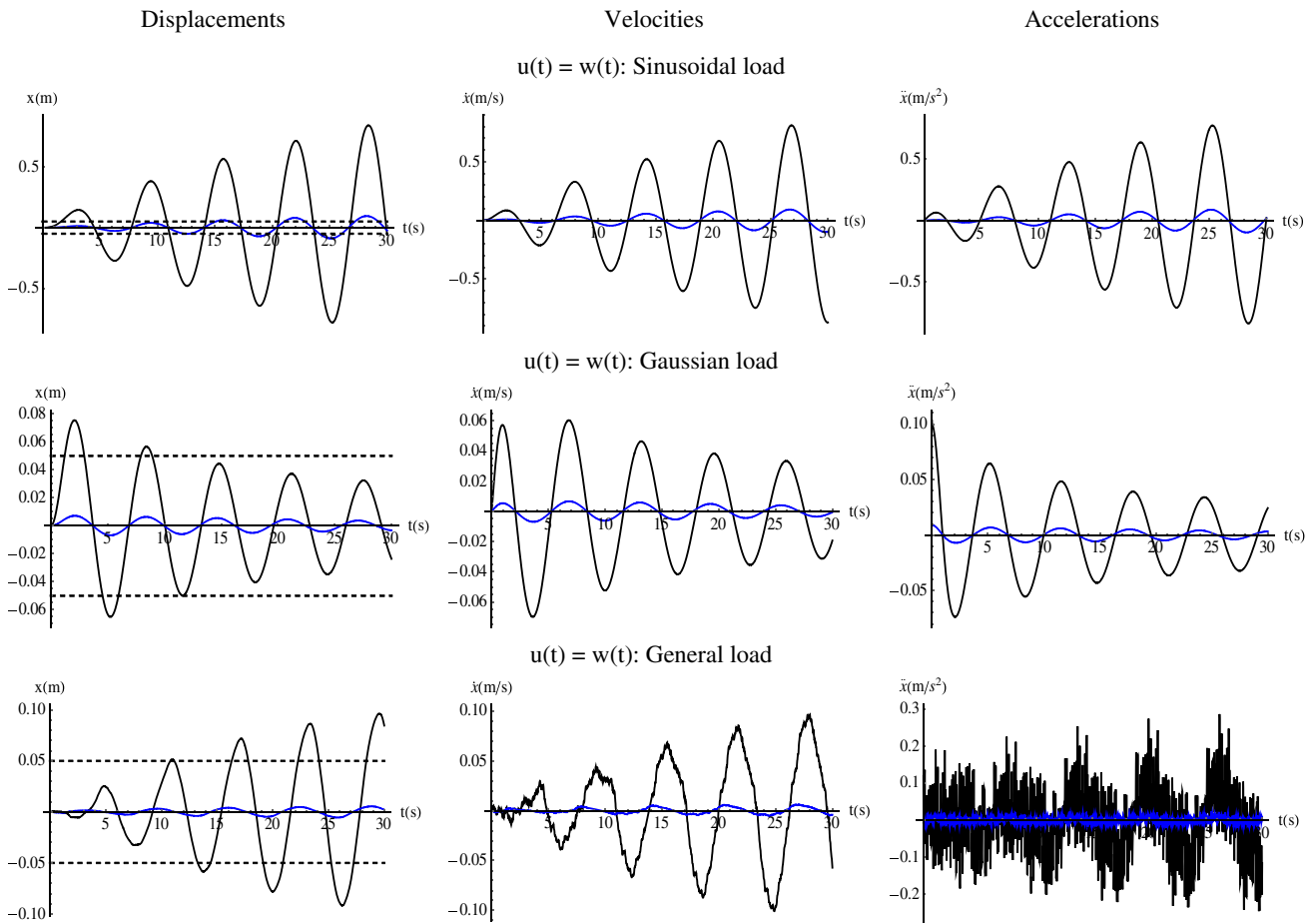
Fig. 9 Response of the structure (blue line) and damper (black line), for $w(t) = u(t) = \{$sinusoidal, Gaussian, general$\}$ and $T_d = 5.99$ s

damper during a motion of 30.0 s (i.e. $t > 25.0$ s as suggested in OPCM (2005)) has been obtained. The goal is to equilibrate the external disturbance $w(t)$ with respect $u(t)$.

Figures 9, 10, and 11 show the TH of the structure (blue curve) and the three dampers (black curve) with $T_d = 5.99$ s when $u(t) = w(t)$, and with $T_d = 6.20$ s, $T_d = 5.71$ s when $u(t) \neq w(t)$. The dashed black lines in the displacement trends represent the blocked threshold assumed of 5.0 cm of the barriers (Fig. 2).

In the acceleration diagrams in Figs. 10 and 11, it is possible to identify better that the damper response follows the adopted $u(t)$, whereas the structure response follows $w(t)$ trend since it acts directly, and with high amplitudes, to the mass m_s as shown in Eq. (16).

Figures 9, 10, and 11 clearly show the reduction of the structure response associated with the SA-TMD configuration. In general, x_d is higher than x_s, as indicated in Chung et al. (2013), since, physically, the damper receives the external loading $w(t)$ and transmits it to the structure with a lower amplitude.

In Fig. 9 where the same external loadings are adopted (i.e. $u(t) = w(t)$), it is possible to note some general considerations. Sinusoidal and general loads increase the response

of the structure and dampers in t, whereas the Gaussian load tends to reduce these responses indicating a better solution. If the peak values are observed at the beginning (e.g. Gauss-Gauss loading), the damping performance in terms of RMS is strongly influenced by these peaks.

However, the good performance on the system under the Gaussian load (Figs. 10 and 11) could be not verified for large period; in fact, from $t > 20.0$ s, the displacements of the damper increase reaching a high value at $t \approx 30.0$ s like the initial amplitude.

In Fig. 9, for the sinusoidal loads with a $w(t)$ frequency of 0.159 Hz, it is possible to see the resonance phenomenon between $w(t)$ and the system; in fact, the maximum displacements (i.e. $x_d \approx 0.90$ m and $x_s \approx 0.10$ m) are verified for this case for $f_d = 0.166$ Hz ≈ 0.159 Hz.

Comparisons and discussions

Figure 12 shows some resumed results where it is possible to see that the damper 3 more reduces the structural response with respect the damper 1 (Fig. 12a). For this, in Fig. 12b, the best results are plotted showing the minimum
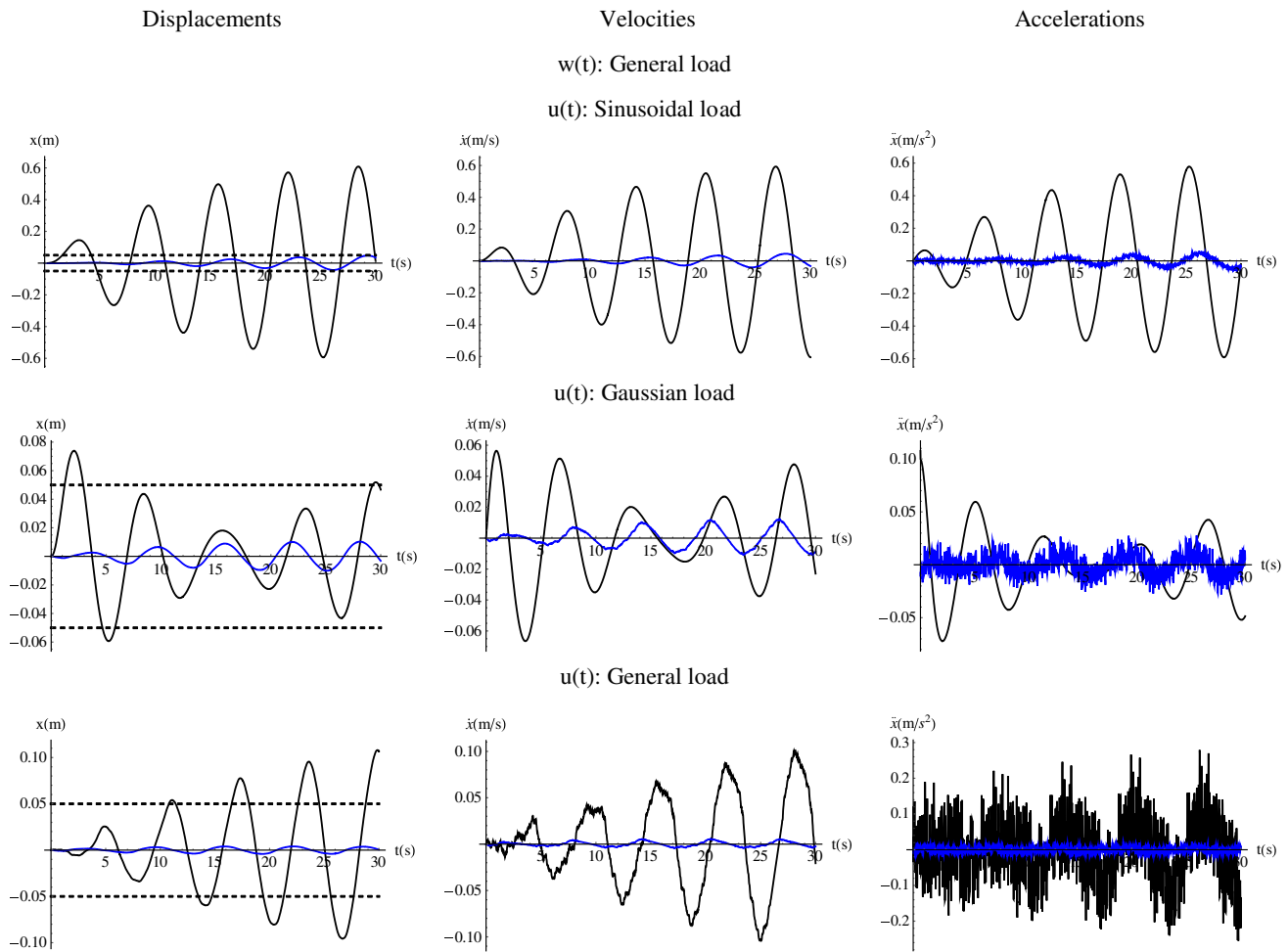
Displacements · · · Velocities · · · Accelerations

w(t): General load

u(t): Sinusoidal load

u(t): Gaussian load

u(t): General load

Fig. 10 Response of the structure (blue line) and damper (black line), for $w(t) = u(t) = \{$sinusoidal, Gaussian, general$\}$ and $T_d = 6.27$ s

values of $x_s \approx 1.0$ cm and $x_s \approx 0.38$ cm for the gen-Gauss and gen-gen combination, respectively.

It is important to note that, by using the same function for $u(t)$ and $w(t)$ loads, the best equilibrium should be expected since the external disturbance $w(t)$ is compensated, in terms of energy, by the variable friction force $u(t)$ (Eq. (9)). However, the use of a general random load for $u(t)$ to equilibrate $w(t)$ could be hazardous since it is intrinsically difficult to control this type of load. For this reason, the gen-Gauss combination is considered the best combination in this study. Also, the gen-Gauss combination provides smaller relative displacements (i.e. $x_s(t) - x_d(t)$) than those obtained for gen-gen combination (see Fig. 13a). This is a positive effect since minimising the relative displacements the integrity of the structure is preserved (Zapateiro et al. 2009).

Figure 13 shows the values of x_s in relation to x_d; in particular, Fig. 13a shows their relative displacements $(x_s(t) - x_d(t))$, whereas Fig. 13b shows their values by loop displacements.

The phase between the curves in Fig. 13a is because $w(t) \neq u(t)$ with different periods. This phase tends to increase for gen-gen combination, whereas for gen-Gauss tends to decrease. In general, when $x_s - x_d > 0$ (i.e. $x_s > x_d$), the structure is subjected to an increasing of displacements (i.e. $x_s \uparrow$), which could be critical if it is not damped; otherwise, when $x_s - x_d < 0$, x_d tends to increase (i.e. $x_d \downarrow$); however, it is also controlled by barriers.

In Fig. 13b, it is possible to see that for gen-gen combination, the damper 1 (solid black curve) follows a trend more linear (i.e. curves more elongated and inclined) with respect the damper 3 where the trends are more circular. This indicates that the maximum x_d values are reached for extreme x_s values. Contrary, for the gen-Gauss combination, damper 1 reaches the maximum x_d value at $x_s \approx 0$ (dashed black curve).

Also, for the gen-Gauss combination, both dampers follow a similar trend probably because a Gaussian load for $u(t)$ provides a more stable response. Both dampers provide quasi-overlapping curves due to a similar randomness of $w(t)$ in terms of energy.
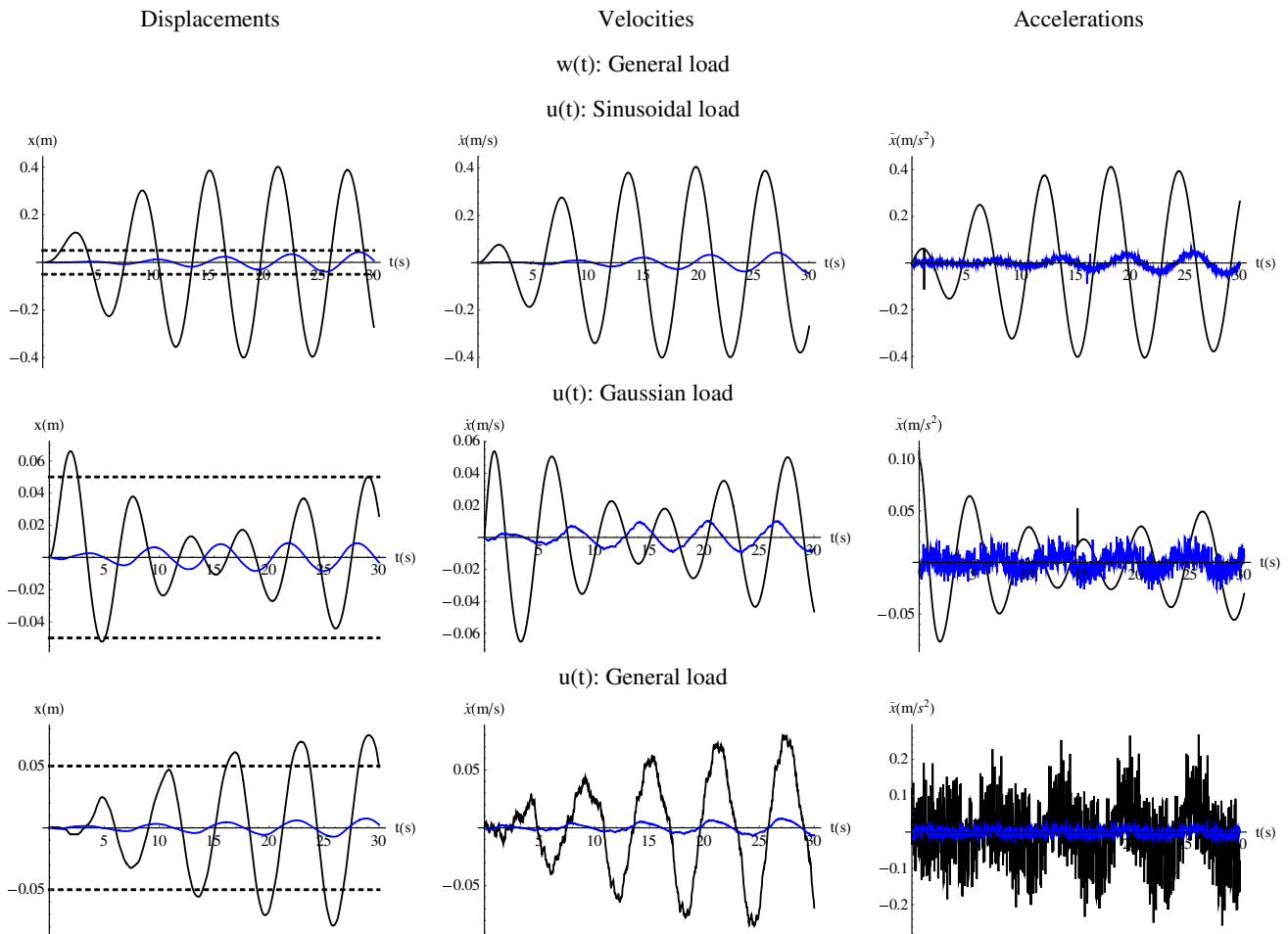
Fig. 11 Response of the structure (blue line) and damper (black line), for $w(t) = u(t) = \{$sinusoidal, Gaussian, general$\}$ and $T_d = 5.71$ s

Figure 14 shows the displacements of the structure and damper 3 and their PDF (Kim and Lee 2019). The amplitude of the PDF for the damper 3 is higher than the PDF for the structure. This means that the structure has a minor variation between the negative and positive displacement peaks, i.e. the curve is sharper when the displacement oscillations are smaller indicating a good control.

Tables 3 and 4 summarise the results in terms of displacements and accelerations for different simulations. Grades from 1 to 3 are assigned to quantify the goodness of the results: (i) for the structure, $x_s < 1.0$ cm (good), $1.0 \leq x_s \leq 4.0$ (fair), and $x_s > 4.0$ cm (poor); (ii) for the dampers, $x_d > 5.0$ cm one time (good), two times (fair), more times (poor). These limits were defined with respect to the adopted barriers threshold of 5.0 cm and previous studies (Table 5).

The results have been compared to the literature as shown in Table 5 and Fig. 15. It is difficult to homogenate the values found in other studies since each structure, even if similar, has its own behaviour. In fact, as mentioned in Ghorbanzadeh et al. (2021), the efficiency of an SA-TMD "depends entirely on the dynamic characteristics of the structure". In this sense, here the criterium of homogenisation regard the absolute response of the non-damped structure, x_{s*}, with respect the damped structure, x_s.

From previous studies where an SA-TMD is applied on a structure, possible efficient values between 0.25 and 0.50 are consistent with this study, i.e. $0.395 \approx 0.318$. In Chung et al. (2011), a high ratio of 0.602 has been estimated since it refers to the response of the SA-TMD with respect to a passive TMD, which corresponds to the contribution of $\mathbb{C}\dot{x}(t)$ in Eq. (1). Actually, by comparing two dampers, the ratio would tend to be 1.0.

Finally, some critical aspects should be mentioned, e.g. for large external excitations, these combinations could not work well. The variation of the structure stiffness should be considered since they can reduce damper efficiency. The used mathematical model does not consider the influences of the high frequencies, modal combinations, non-linear analyses, and soil-structures interactions. Also, it is necessary to consider the site conditions and earthquake characteristics

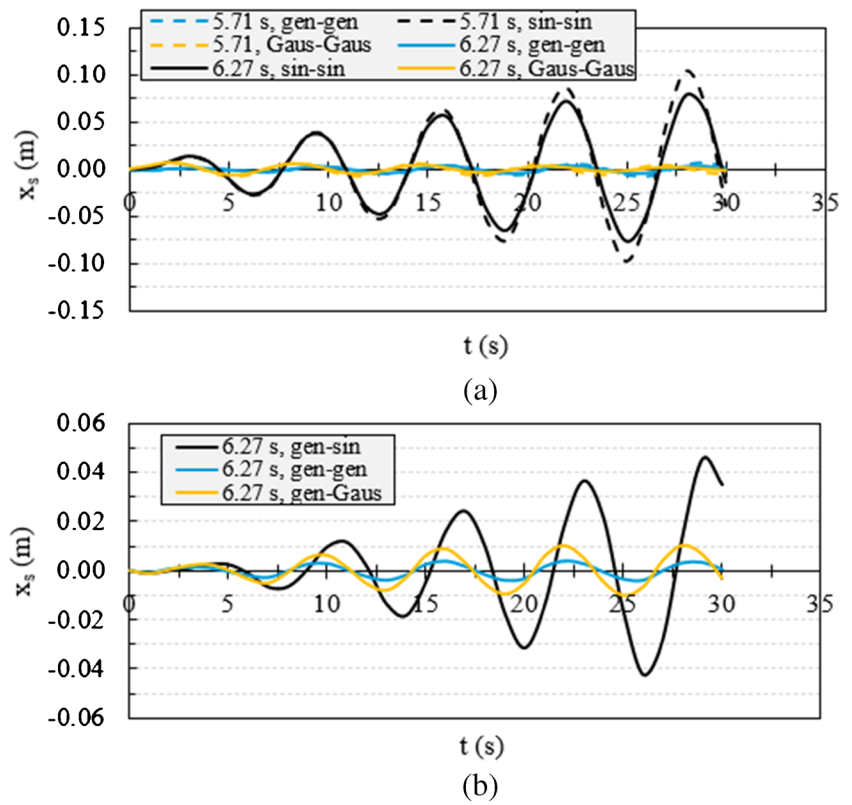**Fig. 12** Resume of some structural displacements x_s for **a** $u(t) = w(t)$ and **b** Fig. 10
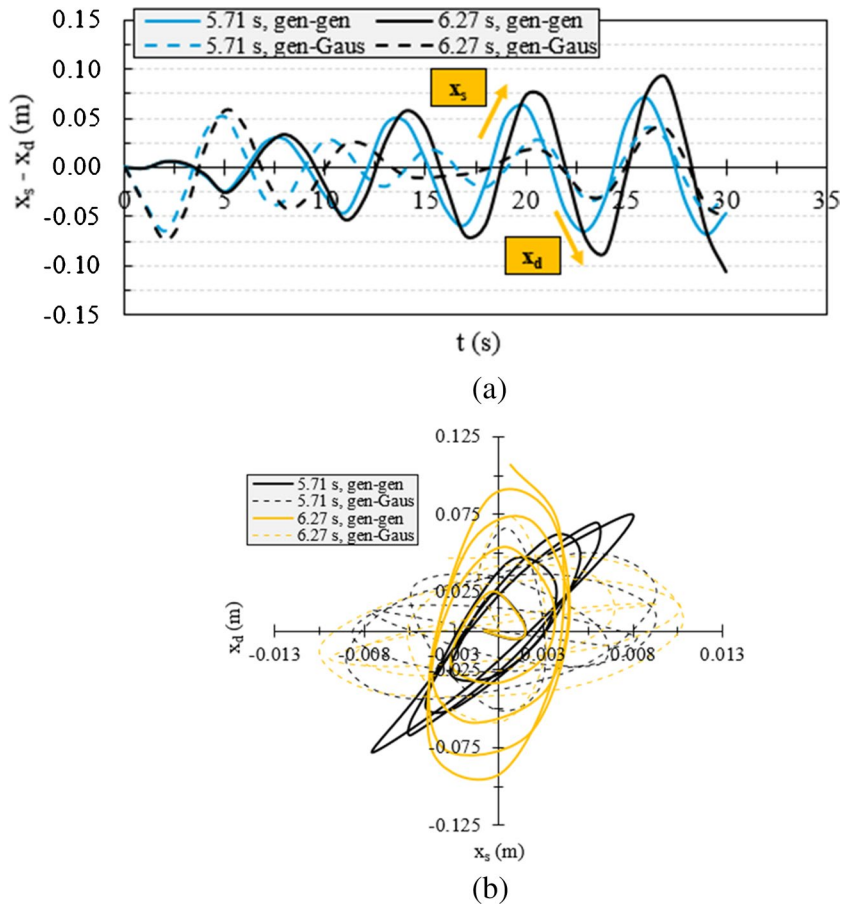

(a)

(b)

Fig. 13 Relative displacements $(x_d(t) - x_s(t))$ plotted **a** in t and **b** by loops
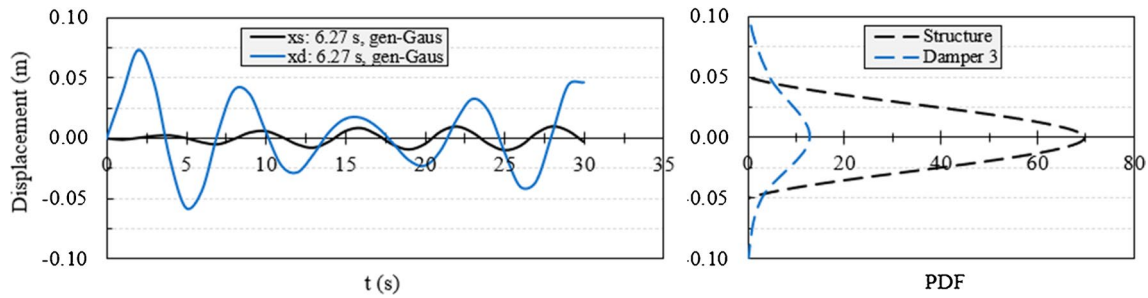

(a)

(b)

Fig. 14 Displacements of the structure (black line) and damper (blue line) and their PDF for $T_d = 6.27$ s and gen-Gauss loading

Table 3 Structural performance assessment (summary results) for $T_d = 5.71$ s

Simulation	Absolute peak x_s (m)	RMS (m)	Absolute peak $\ddot{x}_s$ (m/s^2)	RMS (m/s^2)	Optimization grade (for the structure)	Optimization grade (for dampers)
Gen-gen	0.0075	0.0034	0.0136	0.0065	3	1
Sin-sin	0.1050	0.0475	0.1062	0.0482	1	1
Gaus-Gaus	0.0071	0.0043	0.0090	0.0046	3	2
Gen-sin	0.0402	0.0180	0.0413	0.0186	1	1
Gen-Gaus	0.0088	0.0050	0.0143	0.0065	3	3
Without SA-TMD ($m_d \rightarrow 0$)	0.0826 [a]	-	-	-	N/A	N/A
Infinity SA-TMD ($m_d \rightarrow \infty$)	0.0	-	-	-	N/A	N/A

3 = good. 2 = fair. 1 = poor. *N/A* = not available.

[a] Non-damped structure displacement, x_{s*}

**Table 4** Structural performance assessment (summary results) for $T_d = 6.27$ s

Simulation	Absolute peak x_s (m)	RMS (m)	Absolute peak $\ddot{x}_s$ (m/s^2)	RMS (m/s^2)	Optimization grade (for the structure)	Optimization grade (for dampers)
Gen-gen	0.0039	0.0024	0.0294	0.0106	3	1
Sin-sin	0.0779	0.0391	0.0771	0.0390	1	1
Gaus-Gaus	0.0071	0.0033	0.0090	0.0037	3	2
Gen-sin	0.0457	0.0196	0.0491	0.0190	1	1
Gen-Gaus	0.0102	0.0056	0.0158	0.0071	2	2

Table 5 Displacement reductions with SA-TMD

Reference	x_s/x_{s*} (< 1.0)	Action type for $w(t)$
Chung et al. (2013)	0.429	Sinusoidal and general
Pinkaew and Fujino (2001)	0.250	Sinusoidal
Shih and Sung (2021a)	0.395	General
Lin et al. (2010)	0.50	General
Gu et al. (2002)	0.40	Power spectral density
Mean value	0.395	-
This study (mean)[a]	0.318	-

[a] By using RMS = {0.0475, 0.005} m (see Table 3)

Fig. 15 Comparison of the results (Table 5)
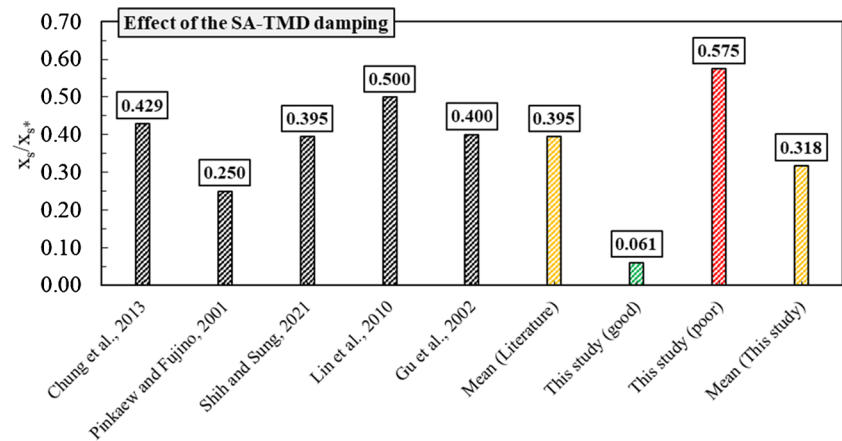
to design well SA-TMDs. These aspects could be future challenges for the authors (Zacchei et al. 2020; Zacchei and Brasil 2022; Zacchei and Lyra 2022).

Conclusions

In this paper, SA-TMDs on a structure under a variable damping model are investigated. The main conclusions are as follows:

1) Numerical analyses have been carried out to simulate several multi-harmonic excitations for external, $w(t)$, and controlled damper, $u(t)$, forces. This approach should capture the seismic input, which is unknown a priori. The goal is to calibrate $u(t)$ in function of $w(t)$. Deterministic and probabilistic data have been adopted to consider different characteristics for dampers (3 dampers on 1 structure) thus their behaviour. The used f_d ranges between 0.159 and 0.175 Hz.

2) In general, $x_d > x_s$ since the damper receives the external loading $w(t)$ and transmits it to the structure with a lower amplitude. Results in Figs. 9, 10, and 11 show that sinusoidal and general loadings increase the response of the structure and dampers in t, whereas the Gaussian loadings tend to reduce these responses. However, the good performance on the system under the Gaussian load could be not verified for large period. Under resonance effects, it is possible to reach values of $x_d \approx$ 0.90 m and $x_s \approx 0.10$ m.

3) The best results are obtained for gen-Gauss and gen-gen combinations with minimum values of $x_s \approx 1.0$ cm and $x_s \approx 0.38$ cm, respectively. Given that the general random load for $u(t)$ to equilibrate $w(t)$ could be difficult to be controlled, the gen-Gauss combination appears the best combination in this study. Also, considering relative displacements $(x_s(t) - x_d(t))$, for this combina-

tion, the phase tends to decrease, and it provides a more stable response. An optimum SA-TMD can reduce the structure displacements up to ~70.0% indicating a good performance in controlling different oscillations.

Finally, the effectiveness of the studied SA-TMD mitigation strategy is very sensitive to the random nature of loadings, which should represent the expected earthquake frequency contents. For this, we hope in the future to carry out experimental campaigns to improve the studied model with other effects such as the influences of the high frequencies, stiffness variations, and real seismic inputs.

Annex A

There is a wide range of anti-seismic devices, which can be divided conceptually in:

1. Isolation a structure with respect to the external forces (e.g. increasing the period or reducing the forces).
2. Damping the energy by adjusting the velocities (e.g. dissipation of controlling velocities).
3. Damping the energy by adjusting the displacements (e.g. dissipation of relative displacements).
4. Stiffening the structure with rigid connections (e.g. changing the behaviour of the structure).

Table 6 lists the classification, description, and some useful values for each anti-seismic device. The first, second, and third devices must support at least 10.0 complete loops. Moreover, their mechanical characteristics, in the loops following the first one, will not vary by more than 15.0% compared to the characteristics during the third loop (OPCM 2005). A general design rule in terms of energy is that the reversibility of stored energy is ≥ 0.25 of the energy dissipated (Medeot 2017).

Table 6 Anti-seismic devices (collected data from Castellano and Infanti (2009); OPCM (2005); SPES (2017); Medeot (2017))

Classification	Sub-classification	Name	Description	Constitutive law (order of magnitude)		
				Force (kN)	Displacement (mm)	Shear strain
Isolators	Elastomeric (rubber)	Elastomeric isolators	They are modelled as linear by effective stiffness, k_e, and equivalent viscous damping ratio ξ_e (10.0–15.0% at 100.0% shear strain). $\xi_e = W_d/(2\pi \times F \times d)$, where W_d, F, and d are the maximum energy, force, and displacement, respectively, corresponding to a complete loop	±150.0	-	±1.50
		Lead rubber bearing	They are modelled as bilinear, linear, or non-linear. ξ_e can be up to 30.0%	±150.0	-	±1.50
	Sliders (steel)	Curved surface sliders	They use gravity as the restoring force. Energy dissipation is provided by friction. The parameters of the bilinear constitutive law depend on the radius of curvature and friction coefficient (between 0 and 4.0%)	±800.0	±400.0	-
		Flat surface sliders	The energy dissipation capacity is very high. The slider with dampers can be free or guided	±3000.0	±80.0	-
Velocity dependent devices	(Cylindrical pistons)	Fluid viscous dampers [a]	They exploit the reaction force of fluids. They are modelled as non-linear by the force–velocity ($F-v$) law: $F = C\,v^{0.15}$, where C is the damping constant	±100.0	±50.0	-
		Fluid spring dampers	The law is $F = F_0 + (K\,x) + (C\,v^{0.15})$, where K is the stiffness, x is the displacement, and F_0 is the pre-load force (to avoid for instance braking forces in bridges)	±1500.0	±150.0	-

Table 6 (continued)

Classification	Sub-classification	Name	Description	Constitutive law (order of magnitude)		
				Force (kN)	Displacement (mm)	Shear strain
Displacement dependent devices	Non-linear (steel)	Steel hysteretic dampers	They use as a source of energy dissipation the hysteretic (stable loops) yielding of steel elements	±300.0	±200.0	-
		Shape memory alloy devices	They are axial restraint devices exploiting the super-elastic properties of alloys. Their behaviour enables to limit the maximum load transmitted to the structure	±20.0	±20.0	-
		Buffers	They are axial devices comprising elastomeric discs. They always are compressed, regardless of the direction of the movement	1600.0	70.0	-
	Linear or quasi-linear (bracing)	Elastomeric viscoelastic dampers	They are strained in shear connecting the moving parts of a structure. The equivalent viscous damping is 15.0 – 20.0% at 100.0% shear strain	±70.0	-	±1.50
Rigid connection devices	Temporary	Shock transmission units	They provide a dynamic connection very stiff. They change the structural behaviour	±2500.0	±8.0	-
	Permanent	Guide bearings and restraint bearings	They provide steady restraint in one or two horizontal directions. They adjust rotations and vertical displacements, and they do not transmit bending moments and vertical loads	3500.0	0.30	-
	Fuse restraints	Mechanical fuse restraints	They prevent relative movement between connected parts up to when a pre-established force is not overpassed. Here, the movements (in one or more direction) are permitted but provoking the breakaway of some components	13000.0	4.0	-

[a]This device can be installed in a tuned mass damper (TMD), which is one such classical passive device

Data availability Data will be made available on request.

Declarations

Conflict of interest The authors declare no competing interests.

References

Abramowitz M, Stegun IA (1965) Handbook of mathematical functions with formulas, graphs, and mathematical tables, Dover Publications, New York, p 1060

Aggumus H, Cetin S (2018) Experimental investigation of semiactive robust control for structures with magnetorheological dampers. J Low Freq Noise, Vib Act Control 37(2):216–234

AutoCAD, Software, Version 2010, Autodesk, Inc., 2010

Anti-seismic devices S00, FIP Industriale SpA. Material retrieved at: Sociedade Portuguesa de Engenharia Sísmica (SPES), Seminário de Verão 2017, 26–27 October 2017. On-line document: https://www.fipindustriale.it/public/S00_DISP-ANTISISMICI-eng.pdf

Bagheri S, Rahmani-Dabbagh V (2018) Seismic response control with inelastic tuned mass dampers. Eng Struct 172:712–722

Bahar A, Pozo F, Acho L, Rodellar J, Barbat A (2010) Hierarchical semiactive control of base-isolated structures using a new inverse model of magnetorheological dampers. Comput Struct 88:483–496

Basili M, De Angelis M, Fraraccio G (2013) Shaking table experimentation on adjacent structures controlled by passive and semi-active MR dampers. J Sound Vib 332:3113–3133

Bekdaş G, Nigdeli SM, Yang XS (2018) A novel bat algorithm based optimum tuning of mass dampers for improving the seismic safety of structures. Eng Struct 159:89–98

Castellano MG, Infanti S (2009) Recent applications of Italian anti-seismic devices. WIT Trans Built Environ 104:333–342

Castellano MG, Indirli M, Matelli A (2001) Progress of application, research and development and design guidelines for shape memory alloy for cultural heritage structures in Italy, PSPIE's 8th Annual International Symposium on Smart Structures and Materials. Newport Beach, CA, USA

Chandiramani NK (2016) Semiactive control of earthquake/wind excited buildings using output feedback. Procedia Engineering 144:1294–1306

Chang CM, Shia S, Lai YA (2018) Seismic design of passive tuned mass damper parameters using active control algorithm. J Sound Vib 426:150–165

Chen PC, Wang SJ (2017) Improved control performance of sloped rolling-type isolation devices using embedded electromagnets. Struct Control Health Monit 24:1853–1869

Chung LL, Yang CY, Chen HM, Lu LY (2011) Study on algorithms for semi-active control of isolation system with variable friction. Procedia Eng 14:974–981

Chung LL, Lai YA, Yang CSW, Lien KH, Wu LY (2013) Semi-active tuned mass dampers with phase control. J Sound Vib 332:3610–3625

Ciampi V, Ciucci M, Guidi G (2009) Sistemi innovativi per la protezione sismica di impianti a rischio di incidente rilevante, Valutazione e Gestione del Rischio negli Insediamenti Civile ed Industriali–VGR2k (Seminary), Pisa, Italy, October 1–12

Dattoli G (2000) Generalized polynomials, operational identities and their applications. J Comput Appl Math 118:111–123

Dattoli G, Torre A, Carpanese M (1998) Operational rules and arbitrary order Hermite generating functions. J Math Anal Appl 227:98–111

European Committee for Standardization (CEN) (2004) Design of structures for earthquakes resistance – Part 1: General rules, seismic actions and rules for buildings, EN 1998–1:2004, Brussel, Belgium

European Committee for Standardization (CEN) (2008) Anti-seismic devices, prEN 15129: Brussel, Belgium

Eason RP, Sun C, Dick AJ, Nagarajaiah S (2013) Attenuation of a linear oscillator using a nonlinear and a semi-active tuned mass damper in series. J Sound Vib 332:154–166

Elias S, Matsagar V (2018) Wind response control of tall buildings with a tuned mass damper. J Build Eng 15:51–60

Fitzgerald B, Sarkar S, Staino A (2018) Improved reliability of wind turbine towers eith active tuned mass dampers (ATMDs). J Fo Sound Vib 419:103–122

Gaul L, Becker J (2014) Reduction of structural vibrations by passive and semi-active controlled friction dampers. Shock Vib 1–7:2014

Gaul L, Albrecht H, Wirnitzer J (2004) Semi-active friction damping of larges space truss structures. Shock Vib 11:173–186

Ghorbanzadeh M, Uygar E, Sensoy S (2021) Lateral soil pile structure interaction assessment for semi active tuned mass damper buildings. Structure 29:1362–1379

Gu M, Chen SR, Chang CC (2002) Control of wind-induced vibrations of long-span bridges by semi-active lever-type TMD. J Wind Eng 90:111–126

Gu X, Yu Y, Li J, Li Y (2017) Semi-active control of magnetorhological elastomer base isolation system utilising learning-based inverse model. J Sound Vib 406:346–362

Gu X, Yu Y, Li J, Li Y (2017b) Semi-active control of magnetorheological elastomer base isolation system utilising learning-based inverse model. J Sound Vib 406:346–362

Hu Z, Su C, Chen T, Ma H (2016) An explicit time-domain approach for sensitivity analysis of non-stationary random vibration problems. J Sound Vib 382:122–139

Hussan M, Rahma MS, Sharmin F, Kim D, Do J (2018) Multiple tuned mass damper for multi-mode vibration reduction of offshore wind turbine under seismic excitation. Ocean Eng 160:449–460

Jabary RN, Madabhushi GSP (2018) Tuned mass damper positioning effects on the seismic response of a solid-MDOF-structure system. J Earthquake Eng 22:281–302

Jiang Z (2018) The impact of a passive tuned mass damper on offshore single-blade installation. J Wind Eng Ind Aerodyn 176:65–77

Kim SY, Lee CH (2018) Optimum design of linear multiple tuned mass dampers subjected to white-noise base acceleration considering practical configurations. Eng Struct 171:516–528

Kim SY, Lee CH (2019) Peak response of frictional tuned mass dampers optimally designed to white noise base acceleration. Mech Syst Signal Process 117:319–332

Lai YA, Yang CSW, Lien KH, Chung LL, Wu LY (2016) Suspension-type tuned mass dampers with varying pendulum length to dissipate energy. Struct Control Health Monit 1–19:2016

Lazarek M, Brzeski P, Perlikowski P (2018) Design and identification of parameters of tuned mass damper with inerter which enables changes of inertance. Mech Mach Theory 119:161–1763

Lin CC, Lu LY, Lin GL, Yang TW (2010) Vibration control of seismic structures using semi-active friction multiple tuned mass dampers. Eng Struct 32:3404–3417

Lorenz M, Heimann B, Härtel V (2006) A novel engine mount with semi-active dry friction damping. Shock Vib 13:559–571

Lu LY, Chung LL, Lin GL (2004) A general method for semi-active feedback control of variable friction dampers. J Intell Mater Syst Struct 15:393–412

Lu Z, Chen X, Zhou Y (2018a) An equivalent method for optimization of particle tuned mass damper based on experimental parametric study. J Sound Vib 419:571–584

Lu Z, Huang B, Zhang Q, Lu X (2018b) Experimental and analytical study on vibration control effects of eddy-current tuned mass dampers under seismic excitations. J Sound Vib 421:153–165

Luzi L, Lanzano G, Felicetta C, D'Amico MC, Russo E, Sgobba S, Pacor F, & ORFEUS Working Group 5, Engineering Strong Motion Database (ESM), Version 2.0, Istituto Nazionale di Geofisica e Vulcanologia (INGV), 2020. https://doi.org/10.13127/ESM.2

Ma J, Dong L, Zhao G, Li X (2019) Ground motions induced by mining seismic events with different focal mechanisms. Int J Rock Mech Min Sci 116:99–110

Maddaloni G, Caterino N, Occhiuzzi A (2017) Shake table investigation of a structure by recycled rubber devices and magnetorheological dampers. Struct Control Health Monit 24:1–17

Medeot R (2017) The European standard on anti-seismic devices, New Zealand Society for Earthquake Engineering (NZSEE), 15th world conference on seismic isolation, energy dissipation and active vibration control of structures, Wellington, New Zealand, pp 27–29

Nagarajaiah S, Sonmez E (2007) Structures with semiactive variable stiffness single/multiple tuned mass dampers. J Struct Eng 67–77:2007

Nagarajaiah S, Varadarajan N (2005) Short time Fourier transform algorithm for wind response control of buildings with variable stiffness TMD. Eng Struct 27:431–441

Oliveira F, Gil de Morais P, Suleman A (2015) Semi-active control of base-isolated structures. Procedia Eng 114:401–409

Ordinanza del Presidente del Consiglio dei Ministri (OPCM) (2005) Norme Tecniche per il Progetto, la Valutazione e l'Adeguamento Sismico degli Edifici, Testo integrato all'Allegato 2 – Edifici – all'Ordinanza 3274 come modificato dall'OPCM 3431 del 3/05/05, Rome, Italy

Pinkaew T, Fujino Y (2001) Effectiveness of semi-active tuned mass dampers under harmonic exitation. Eng Struct 23:850–856

Salvi J, Pioldi F, Rizzi E (2018) Optimum tuned mass dampers under seismic soil-structure interaction. Soil Dyn Earthq Eng 114:576–597

Sanchez WHC, Linhares TM, Neto AB, Fortaleza ELF (2017) Passive and semi-active heave compensator: project design methodology and control strategies. PLoS ONE 12(8):1–26

Shi W, Wang L, Lu Z, Gao H (2018a) Study on adaptive-passive and semi-active eddy current tuned mass damper with variable damping. Sustainability 10:99–117

Shi W, Wang L, Lu Z, Zhang Q (2018b) Application of an artificial fish swarm algorithm in an optimum tuned mass damper design for a pedestrian bridge. Appl Sci 8:175–189

Shih MH, Sung WP (2021a) Parametric study of impulse semi-active mass damper with developing directional active joint. Arab J Sci Eng 1–19:2021

Shih MH, Sung WP (2021b) Seismic resistance and parametric study of building under control of impulsive semi-active mass damper. Appl Sci 11:1–26

Shuliang C, Yajun X, Yanwu W (2011) Semi-active control of base isolation with energy transition control device. Procedia Eng 15:85–89

Su C, Xu R (2014) Random vibration analysis of structures by a time-domain explicit formulation method. Struct Eng Mech 52(2):239–260

Sun C, Jahangiri V (2018) Bi-directional vibration control of offshore wind turbines using a 3D pendulum tuned mass damper. Mech Syst Signal Process 105:338–360

Trikande MW, Jagirdar VV, Rajamohan V, Sampat Rao PR (2017) Investigation on semi-active suspension system for multi-axle armoured vehicle using co-simulation. Def Sci J 67(3):269–275

Van Til J, Alijani F, Voormeeren SN, Lacarbonara W (2019) Frequency domain modelling of nonlinear end stop behaviour in tuned mass dampers systems under single- and multi-harmonic excitations. J Sound Vib 438:139–152

Wang W, Wang X, Hua X, Song G, Chen Z (2018a) Vibration control of vortex-induced vibrations of a bridge deck by a single-side pounding tuned mass damper. Eng Struct 173:61–75

Wang YR, Feng CK, Chen SY (2018b) Damping effects of linear and nonlinear tuned mass dampers on nonlinear hinged-hinged beam. J Sound Vib 430:150–173

Wang L, Nagarajaiah S, Shi W, Zhou Y (2021) Semi-active control of walking-induced vibrations in bridges using adaptive tuned mass damper considering human-structure-interaction. Eng Struct 244:1–15

Wen B, Moustafa MA, Junwu D (2018) Seismic response of potential transformers and mitigation using innovative multiple tuned mass dampers. Eng Struct 174:67–80

Wolfram Mathematica (2017) Software, Version 11 Student Edition, Wolfram Research, Inc

Wu LY, Chung LL, Wu CH, Huang HH, Lin KW (2011) Vibrations of nonlocal Timoshenko beams using orthogonal collocation method. Procedia Eng 14:2394–2402

Wu Q, Zhao W, Zhu W, Zheng R, Zhao X (2018) A tuned mass damper with nonlinear magnetic force for vibration suppression with wide frequency range of offshore platform under earthquake loads. Shock Vib 1–18:2018

Xia Z, Wang W, Hou J, Wei S, Fang Y (2016) Non-linear dynamic analysis of double-layer semi-active vibration isolation systems using revised Bingham model. J Low Freq Noise, Vib Act Control 35:17–24

Yari A, Mirnia M (2021) Direct method for solution variational problems by using Hermite polynomials. Bol Soc Paran Mat 39:223–237

Zacchei E, Brasil R (2022) A new approach for physically based probabilistic seismic hazard analyses for Portugal. Arab J Geosci 15:1–22

Zacchei E, Lyra P (2022) Recalibration of low seismic excitations in Brazil through probabilistic and deterministic analyses: application for shear buildings structures. Struct Concr 1–19:2022

Zacchei E, Nogueira CG (2021) 2D/3D numerical analyses of corrosion initiation in RC structures accounting fluctuations of chloride ions by external actions. KSCE J Civ Eng 25:2105–2120

Zacchei E, Molina JL, da Fonseca Rebello, Brasil RM (2017) Seismic hazard assessment of arch dams via dynamic modelling: an application to the Rules Dam in Granada, SE Spain. Int J Civil Eng 2017:1–10

Zacchei E, Molina JL, Brasil RM (2017) Nonlinear degradation analysis of arch-dam blocks by using deterministic and probabilistic seismic input. J Vib Eng Technol 2018:1–13

Zacchei E, Lyra P, Stucchi F (2020) Pushover analysis for flexible and semi-flexible pile-supported wharf structures accounting the dynamic magnification factors due to torsional effects. Struct Concr 21:1–20

Zapateiro M, Karimi HR, Luo N, Phillips BM, Spencer Jr BF (2009) A mixed H_2/H_∞-based semiactive control for vibration mitigation in flexible structures, Joint 48th IEEE Conference on Decision and Control and 28th Chinese Control Conference, Shanghai, P.R., China, pp 2186–2191